Acta Materialia 247 (2023) 118740

Contents lists available at ScienceDirect

Acta Materialia

journal homepage: www.elsevier.com/locate/actamat

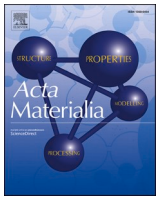

Full length article

The brittle-to-ductile transition in aluminosilicate glasses is driven by topological and dynamical heterogeneity

Longwen Tang [a], Morten M. Smedskjaer [b], Mathieu Bauchy [a,*]

[a] Department of Civil and Environmental Engineering, Physics of AmoRphous and Inorganic Solids Laboratory (PARISlab), University of California, Los Angeles, CA 90095, USA
[b] Department of Chemistry and Bioscience, Aalborg University, Aalborg 9220, Denmark

ARTICLE INFO

Keywords:
Molecular dynamics simulations
Brittle-to-ductile transition
Non-metallic glasses
Heterogeneity
Topological constraint theory

ABSTRACT

Amorphous materials can exhibit varying degrees of nanoscale ductility depending on their atomic structure. Despite its critical importance for applications, the physical origin that controls ductility remains largely unknown. Here, by using molecular dynamics simulations, we investigate the ductile-to-brittle transition of oxide glasses as a function of the connectivity of the atomic network. Interestingly, based on topological constraint theory, we show that the structural origin of the ductile-to-brittle transition is the rigidity transition caused by the percolation of stressed-rigid atomic clusters. Our further analysis of four-point correlation functions reveals that, similar to the case of supercooled liquids, the plastic dynamics of oxide glasses at room temperature are strongly correlated and spatially heterogeneous. Surprisingly, the dynamical length scale of plastic events significantly decreases when the stressed-rigid cluster percolates, resulting in a narrower transient plastic rearrangement region. These results provide physical insights into the relationship between the topological features of atomic structure, fracture behavior, and stress-induced dynamical heterogeneity of glasses.

1. Introduction

Under mechanical loading, glasses can break in quite different ways, namely, brittle fracture triggered by catastrophic propagation of cracks and ductile fracture dominated by the obvious plastic deformation. The ductile-to-brittle transition can be observed for various types of glasses depending on their structure in both experiments and simulations [1–5]. Understanding the relationship between structural features and fracture behavior of glasses is of critical importance for both condensed matter physics and materials science [6–8]. For crystalline materials, ductility is typically controlled by the motion of dislocations, which results in the formation of macroscopic shear bands [9–11]. This behavior is different from that of glasses due to their lack of long-range order, as the basic plastic event in glasses is usually identified as local rearrangement rather than dislocation [12]. To establish the structure-properties relationship, various types of structural features that can be correlated with plastic events in glasses have been proposed in recent years [4,13–16]. Although these structural predictors can capture the propensity for the rearrangement location, the structure-property relationship obtained from these approaches is local and hence, lacks the description of the rearrangements and corresponding interactions that occur at a larger length scale.

Since glasses are out-of-equilibrium materials, the spatial heterogeneity of the local chemical and structural environment becomes prominent due to the fluctuation [17,18]. As a result, nontrivial length scales emerge, which are believed to play an important role in the abnormal dynamical behavior of amorphous materials, including the dramatic increase of the relaxation time when approaching the glass transition [17,19] and jamming transitions [20,21]. However, the dynamical heterogeneity of plastic events in glasses driven by mechanical loading remains elusive [7].

Topological constraint theory (TCT), or rigidity theory, provides a path to understand the important role of atomic structure on the mechanical behavior of amorphous material. According to this theory, the complex atomic networks in glasses can be simplified as a network of constraints, in which the chemical interaction between atoms is treated as a mechanical truss [22–24]. Following Maxwell's stability theory [25], the constraints network can be classified into three categories, namely, flexible, stressed-rigid, and isostatic. For the flexible state, the network has internal degrees of freedom that lead to floppy modes [26].

Abbreviations: TCT, Topological constraint theory; BO, Bridging oxygen; NBO, Non-bridging oxygen.

* Corresponding author.
E-mail address: bauchy@ucla.edu (M. Bauchy).

https://doi.org/10.1016/j.actamat.2023.118740
Received 28 October 2022; Received in revised form 23 January 2023; Accepted 31 January 2023
Available online 3 February 2023

On the contrary, in the stressed-rigid state, the network is overconstrained and eigen-stress becomes prominent [27,28]. Between the above two states, the isostatic state is achieved when the network is rigid but free of eigen-stress. More importantly, recent work shows that various anomalous properties and dynamics of glasses emerge in the isostatic state [29–32]. Beyond this, TCT can be used to predict the mechanical properties of glasses [33,34] and has been successfully used to design a commercial cover glass, namely Corning® Gorilla® Glass 3 [35–37]. However, most of the previous studies have focused on the macroscopic average number of constraints without carefully considering the effect of the heterogeneous nature of constraints [18]. Nevertheless, recent research suggests that, besides the average number of constraints, the spatial heterogeneity of topological constraints also plays an important role in crack propagation [38].

Here, we investigate the ductile-to-brittle transition in a series of aluminosilicate glasses with varying compositions based on molecular dynamics simulations. From the viewpoint of TCT, we find that a maximum resistance to fracture is achieved when the glass exhibits an optimal, isostatic spatial distribution of its network topology—featuring a percolation of rigid clusters, but a non-percolated distribution of stressed clusters. Combining the analysis of susceptibility and the four-point correlation function, we find an unexpected linkage between dynamic heterogeneity of plastic events and static network connectivity (i.e., before any load is applied). Based on these results, we establish the physical picture that the topology of their atomic networks governs the ductile-to-brittle transition of oxide glasses through the intensity of dynamical heterogeneity.

2. Methods

2.1. Preparing samples

The aluminosilicate glass systems for fracture simulations contained around 35,000 atoms in a slab with dimensions of ~ 150 Å (x) x 110 Å (y) x 36 Å (z) (varied according to the composition). Periodic boundary conditions are applied in all directions. To construct these samples, a small cube (containing around 3000 atoms) is melted at 5000 K for 0.5 ns to lose its initial memory and then cooled to 300 K with a cooling rate of 10^{12} K/s by using a Nosé-Hoover thermostat [39,40]. Afterward, the final simulation sample is constructed by replicating the small cube, following further relaxation at 300 K for 0.5 ns. To induce stress concentration, we create an initial ellipsoidal notch with a length of 5 nm by manually removing the atoms within the region (see Fig. 1e). The position of the ellipsoidal notch is slightly adjusted to ensure charge neutrality. During the above processes, the *NPT* ensemble with a fixed zero pressure is used. A constant time step of 1 fs is selected for all simulations. The interaction between atoms is described by the potential parameterized by Jakse et al. [41], which captures well the atomic structure of aluminosilicate glasses [42]. To obtain statistically meaningful results, we prepare nine independent samples for each composition for the following simulations and analyses. All the simulations are performed by using LAMMPS package [43].

2.2. Fracture simulations

The uniaxial tensile fracture simulation is performed by stretching the box in the y-direction at 300 K, while the box size is fixed in the other

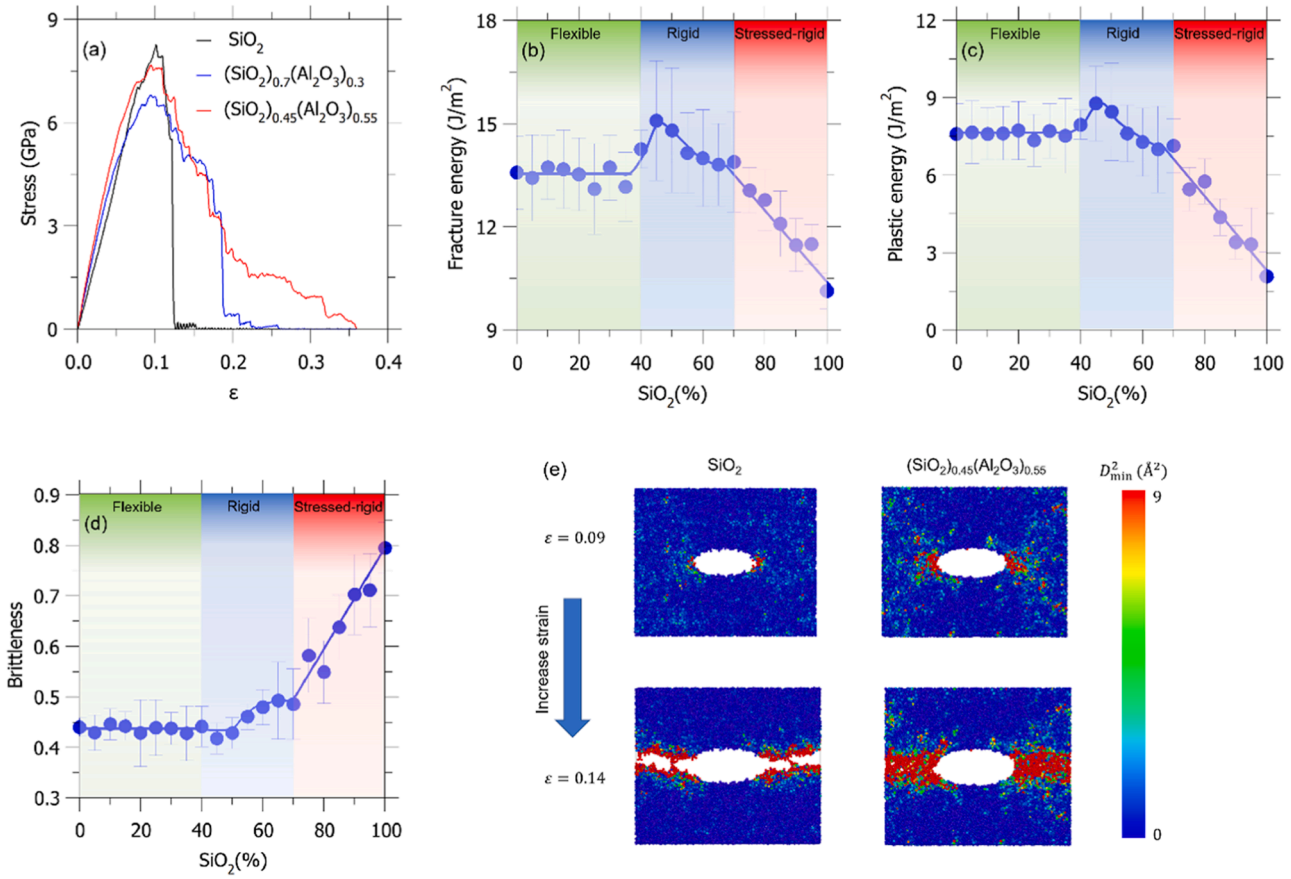

Fig. 1. *Evidence of the brittle-to-ductile transition.* (a) Stress-strain curves of selected aluminosilicate glass compositions. (b–d) Effect of the SiO_2 fraction on the (b) fracture energy, (c) plastic energy, and (d) brittleness of the aluminosilicate glasses. The lines are guides the eye. (e) Contour plots of non-affine square displacement for the selected compositions at strains values of $\varepsilon = 0.09$ and $\varepsilon = 0.14$, respectively.

directions. The strain rate is fixed at 10^8 /s for all fracture simulations. The *NVT* ensemble is used during the simulations. The total fracture energy G_F is obtained by integrating the stress-strain curve. Similarly, the estimated elastic energy G_E is calculated by integrating the stress-strain curve before the peak stress is achieved [44]. Then, the brittleness index B is defined as $G_E/\ G_F$. The non-affine displacement is calculated based on the approach proposed in ref. [12]. In addition to the fracture simulation under 300 K, we also perform the athermal fracture simulation to investigate the influence of temperature fluctuation (see supplementary materials for more details).

2.3. Average number of constraints

We calculate the average number of constraints per atom (n_c) of the basic polytope units in the network, which consists of a cation (i.e., Si or Al) and its neighboring oxygen atoms (i.e., the oxygen atoms within the 2 Å cutoff). In this study, two types of constraints are considered: (i) radial bond-stretching constraints created by Al–O and Si–O bonds (which maintain the distance between pairs of atoms fixed around their average value) and (ii) angular bond-bending constraints associated to Si–O–Si, O–Si–O, and Al–O–Si angles (which maintain the angles between triplets of atoms fixed around their average value). In detail, we first enumerate all the constraints associated with each basic unit. The number of constraints per atom n_c can be calculated as:

$$n_c = \frac{n_{BB} + n_{BS} + 0.5\left(n_{BB}^{shared} + n_{BS}^{shared}\right)}{N} \quad (1)$$

where n_{BB} and n_{BS} represent the numbers of bond-bending and bond-stretching constraints within the polytope, n_{BB}^{shared}, n_{BS}^{shared} the corresponding shared constraints (i.e., in between two neighboring polytopes, and N is the number of atoms in the basic unit.

To analyze the topological heterogeneity of the atomic network, the spatially-connected basic units featuring the same n_c value are identified as a cluster. A cluster is regarded as "rigid" when it includes both $n_c > 3$ and $n_c = 3$ basic units (i.e., $n_c \geq 3$), while a cluster is defined as "stressed-rigid" if only contains stressed-rigid basic units (i.e., $n_c > 3$).

2.4. Dynamical heterogeneity analysis

In the dynamical heterogeneity analysis, we follow the procedure used in refs. [20,45,46]. To understand the nature of microscopic rearrangements while filtering out any stress concentration effect, the analysis is conducted on notch-free samples. First, for each sample without the notch, we perform the uniaxial tensile deformation with the same strain rate as in the fracture simulations in the *x*-, *y*-, and *z*-directions, respectively (i.e., 27 independent simulations are performed for each composition). Then, we calculate the square non-affine displacement $D^2_{min}(\varepsilon)$ for each atom as a function of strain ε [12]. For the calculation of the overlap function Q, the cutoff D_0 is selected as $9Å^2$. Then, the susceptibility χ_4 can be defined as,

$$\chi_4(\varepsilon) = \frac{V}{N^2}\left(\langle Q(\varepsilon)^2\rangle - \langle Q(\varepsilon)\rangle^2\right)$$

where V is the volume of the system and N is the total number of atoms. Note that the temperature term is removed since the temperature remains the same for all compositions. Here, we use the self-part of the four-point correlation function g_4 since we only focus on the plastic events,

$$g_4(r,\varepsilon) = \frac{1}{N\rho}\left\langle \sum_{ij}\delta\left(r - r_j(0) + r_i(0)\right)w\left(D^2_{min}\right)\right\rangle - \left\langle \frac{Q(\varepsilon)}{N}\right\rangle^2$$

where ρ is the density. Thus, the four-point correlation length ξ_4 can be obtained by fitting the envelope line of g_4 [20,45,46], i.e., $g_4(r,\varepsilon_{max}) \propto \exp(-r/\xi_4)$.

3. Results

3.1. Evidence of the brittle-to-ductile transition

We focus on the brittle-to-ductile transition of aluminosilicate glasses (i.e., $(SiO_2)_x(Al_2O_3)_{1-x}$) driven by composition. To this end, we perform uniaxial tensile simulations of these melt-quenched samples based on molecular dynamics simulations (see Method for details). Fig. 1a shows the stress-strain curves of selected compositions upon uniaxial tensile fracture. We observe that, for the pure silica glass, the stress-strain curve exhibits a sudden drop after reaching the peak stress, which indicates a brittle fracture behavior. In contrast, when a certain amount of Al_2O_3 is added (i.e., $(SiO_2)_{0.45}(Al_2O_3)_{0.55}$), the stress-strain curve features a significant "softening" stage (i.e., slow decay of stress after the crack initiates), which suggests a more ductile fracture behavior. We then further calculate the fracture energy and plastic energy to quantify the degree of ductility. To get a statistically reliable result, we perform nine independent uniaxial tensile fracture simulations for each composition. As shown in Fig. 1b and c, for both the fracture energy and plastic energy, the maximum value is achieved at 45% SiO_2 fraction (i.e., $(SiO_2)_{0.45}(Al_2O_3)_{0.55}$). Meanwhile, the sudden drop of the fracture energy and plastic energy occurs when the SiO_2 fraction is larger than 70%. It should be noted that this trend is consistent with the recent experimental results, which suggest the highest crack resistance is reached at around 40% SiO_2 fraction. However, for the Al_2O_3-rich compositions (i.e., SiO_2 fraction less than 40%), no significant difference can be observed.

To quantitatively identify the brittle-to-ductile transition, we compute the brittleness (i.e., the ratio between the elastic energy and fracture energy) for each composition, where a lower value of brittleness indicates higher ductility and vice versa. As shown in Fig. 1d, the brittleness maintains at a low level (around 0.44) until the SiO_2 fraction is larger than 40%. From 50% to 65% SiO_2 fraction, we observe a slight increase of brittleness with SiO_2 fraction. Then, the brittleness sharply increases when the SiO_2 fraction is larger than 70% and reaches a value of 0.8 for pure silica.

We then investigate the mechanism of the brittle-to-ductile transition that occurs at around 70% SiO_2. To this end, we compute the atom's non-affine square displacement, which has been widely used to identify the plastic events in amorphous materials [5,12,13,47]. Fig. 1e shows the contour plots of the non-affine square displacement at different strains. For pure silica, the plastic region is limited to the narrow band attached to the fracture surface. However, in the case of the $(SiO_2)_{0.45}(Al_2O_3)_{0.55}$ composition, the width of the plastic region reaches around 20 Å, which provides resistance to crack propagation at high strain. This result suggests that, for the studied oxide glasses, the toughening mechanism is related to the increase of the typical size of the plastic region that occurs during the whole fracture process.

3.2. Rigidity transition

Next, we attempt to unveil the structural origin of the brittle-to-ductile transition. To this end, we first calculate the average number of constraints n_c (i.e., the number of rigid bonds and angles per atom) that is relevant to the fracture (see Method for details). The key idea of TCT is that we define the basic unit as the cation (i.e., Si and Al) connected by the oxygen neighbors, which are marked as bridging oxygen (BO) or non-bridging oxygen (NBO) according to their local environment. Considering the fact that Al–O bonds are less directional than their Si–O counterparts, Al tetrahedra are less rigid than Si ones (see ref. [42] for more discussion) . As such, Al–O–Al and O–Al–O angles are considered floppy and do not contribute to the number of bond-bending constraints. As shown in Fig. 2a–c, the basic units are identified as flexible ($n_c < 3$), isostatic ($n_c = 3$), or stressed-rigid ($n_c > 3$) according to the average number of constraints per atom in each unit. As a result, Al tetrahedra are considered as flexible basic units, while Si tetrahedra are

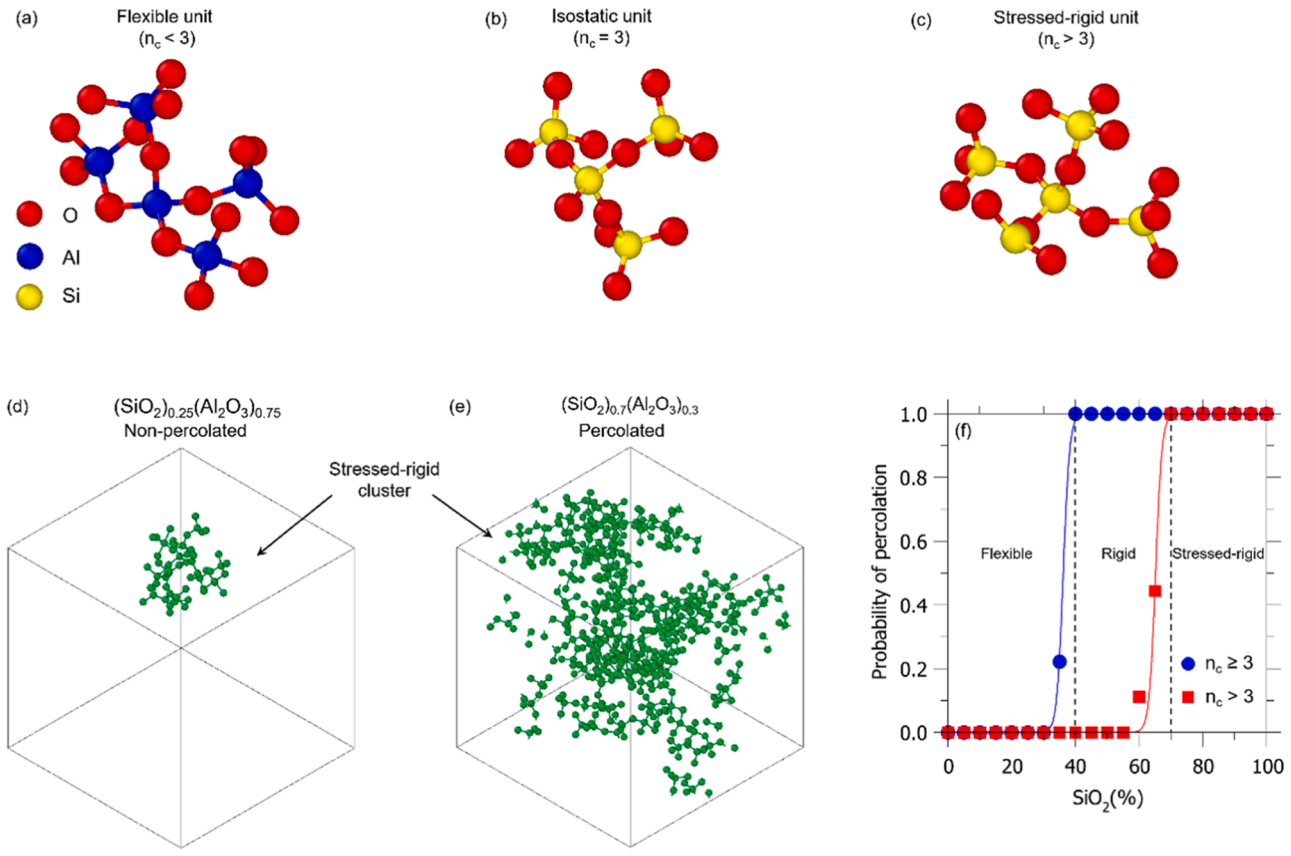

Fig. 2. *Composition-induced percolation of the stressed-rigid cluster*. (a–c) Schematic illustrations of (a) flexible, (b) isostatic, and (c) stressed-rigid units. (d,e) Size of the largest stressed-rigid cluster in the (d) non-percolated and (e) percolated systems. (f) Probability of the percolation as the function of the composition.

regarded as rigid basic units.

Then we perform cluster analysis to distinguish two types of clusters. The cluster is constituted by the spatial connected basic units (i.e., a piece of the network) that have similar features defined as follows. One is defined as the rigid cluster that includes both isostatic and stressed-rigid (i.e., $n_c \geq 3$), while the other is defined as the stressed-rigid cluster wherein the basic units are only stressed-rigid (i.e., $n_c > 3$). Fig. 2d and e show the largest stressed-rigid cluster of the selected compositions. A clear percolation of the stressed-rigid cluster can be observed for $(SiO_2)_{0.7}(Al_2O_3)_{0.3}$, while the sample with a lower SiO_2 fraction (i.e., $(SiO_2)_{0.25}(Al_2O_3)_{0.75}$) only shows a small unpercolated stressed-rigid cluster. To quantitatively identify the percolation, we calculate the probability of percolation of the largest clusters as a function of composition. As shown in Fig. 2f, with the increase in the fraction of the stronger network former (i.e., SiO_2), the sudden percolation of stressed-rigid occurs once the SiO_2 fraction reaches 70%. For the rigid cluster, the results show a similar tendency but the percolation threshold is found at only around 40%, which is significantly lower than for the stressed-rigid one. This difference in percolation thresholds for rigid and stressed-rigid clusters agree with predictions from the self-organization model [28]. According to the observed percolation thresholds, we can divide the composition space into three regions, namely, flexible (SiO_2 fraction < 40%), rigid (40% < SiO_2 fraction < 70%), and stressed-rigid regions (SiO_2 fraction > 70%), respectively.

More importantly, we find that these three regions correspond to the three stages shown in Fig. 1b–c. In the flexible region, the fracture energy and plastic energy remain constant, while the brittleness index maintains a minimum value. The highest fracture energy and plastic energy values are obtained in the rigid region, where only the percolation of the rigid cluster occurs. Interestingly, we also observe that the sudden drop of fracture energy and plastic energy, as well as the sudden increase of brittleness, all occur when the stressed-rigid clusters start to percolate.

3.3. Evolution of the dynamical length scale

To explore the dynamical origin of the brittle-to-ductile transition, we employ the concepts of susceptibility and four-point correlation function [48] as this allows us to quantify the intensity of dynamical heterogeneities. The following analysis is based on the notch-free simulations so as to avoid any spurious effect resulting from the localized stress concentration induced by a notch (see Method Section for more details). Note that, in this study, we only consider the dynamics that are associated with plastic events and we therefore rewrite the self-part of the overlap function as: $Q(\varepsilon) = \sum_{i=1}^{N} w(D^2_{\min})$, where $D^2_{\min}$ is non-affine square displacement. $w(D^2_{\min})$ is 1 when $D^2_{\min} \leq D_0$ and 0 when $D^2_{\min} > D_0$. $Q(\varepsilon)$ represents the number of atoms that experience significant rearrangement at the current strain ε. Fig. 3A shows the computed $Q(\varepsilon)$ curve of the selected compositions. They all show a similar tendency, starting with a minor decrease at a small strain (i.e., nucleation stage), but the Q value then rapidly drops at a specific point (i.e., rapid growth stage) and converges to a non-zero value (i.e., fully fractured stage). For the pure silica glass, the Q value converges at a relatively small strain of ~0.35, while the Q value of $(SiO_2)_{0.45}(Al_2O_3)_{0.55}$ converges at a much larger strain of ~0.5. It should be noted that the failure strain in this analysis is much smaller compared with that in Fig. 1a due to the relatively small system size.

We then move to the susceptibility of Q (i.e., χ_4), which reflects the number of atoms that rearrange together (see Method section for details). Interestingly, as shown in Fig. 3b, for all compositions, χ_4 reaches the maximum values in the final fully fractured stage at $\varepsilon = \varepsilon_{max}$, which indicates that the largest cooperative rearrangement occurs immediately

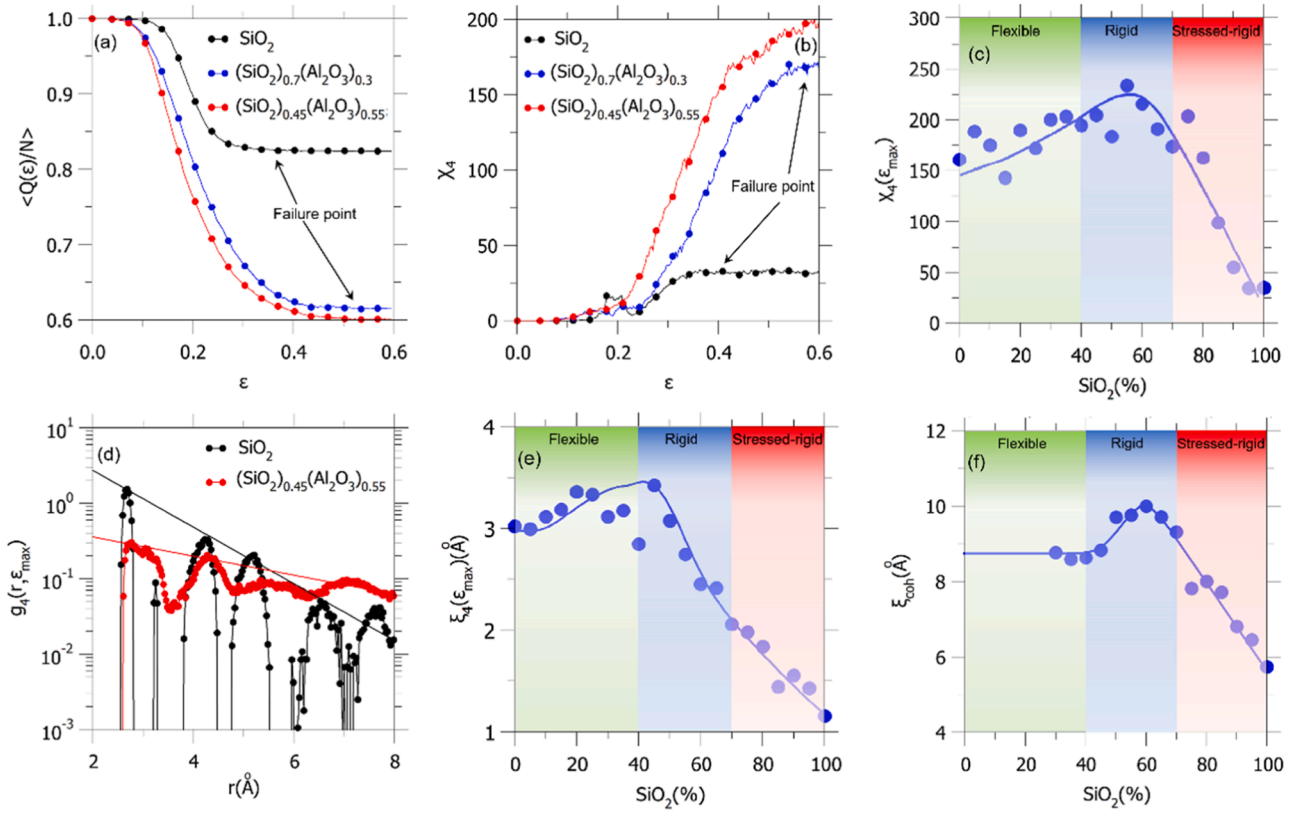

Fig. 3. *Dynamical length scale controlled by the rigidity transition.* (a) Normalized overlap function Q and (b) susceptibility χ_4 as the function of strain ε for selected compositions. (c) χ_4 as a function of composition. (d) Four-point correlation function g_4 curves at strain ε_{max}, which results in the maximum χ_4. The solid line represents the exponent fitting. (e) Extracted four-point correlation length ξ_4 and (f) coherent length ξ_{coh} as a function of composition. The solid lines in Figs. (c), (e), and (f) are used to guide the eye.

before the crack propagates through the sample. Fig. 3c shows the maximum χ_4 value (i.e., $\chi_4(\varepsilon_{max})$) plotted as a function of composition, revealing a similar tendency as that observed for fracture energy and plastic energy in Fig. 1b and 1c, respectively. That is, in the stressed-rigid region, $\chi_4(\varepsilon_{max})$ drops significantly with SiO_2 fraction, while the maximum value is observed in the rigid region.

Furthermore, we identify the dynamical length ξ_4 from the four-point correlation function g_4 following a similar process as proposed in refs. [20,45,46]. That is, ξ_4 is obtained by fitting the envelope line of g_4 (see Method for details). Fig. 3d shows g_4 as the function of the distance between two selected atoms. g_4 decreases faster for pure silica as compared with $(SiO_2)_{0.45}(Al_2O_3)_{0.55}$. Interestingly, we find that ξ_4 sharply decreases with the SiO_2 fraction in the stressed-rigid region, while it obtains the maximum value in the rigid region (Fig. 3e). There is only a minor change of ξ_4 in the flexible region.

We then consider the evolution of the static length due to the change in the connectivity of the atomic network. To this end, we compute the coherent length ξ_{coh} of SiO_2 cluster, which is obtained from the width of the first sharp diffraction peak for Si-O for each composition. Fig. 3f shows the evolution of ξ_{coh} as a function of composition. We find that the evolution of ξ_{coh} follows a similar tendency as that of χ_4, namely, ξ_{coh} exhibits a minimum value for pure silica and increases with the fraction of Al_2O_3 until the maximum value is observed in the rigid region. It should be noted that the above conclusion is still valid under the athermal condition (see supplementary materials for more details).

4. Discussion

We first discuss the linkage between the fracture energy and atomic connectivity of the investigated aluminosilicate glasses. In general, the fracture energy of materials can be divided into contributions from cohesion and plastic events. Unlike the case in crystalline materials, the plasticity of aluminosilicate glasses manifests itself by some local reorganizations, including coordination number changes and bond switching [49], bond breaking, and changes in the shape of ring structures [50,51]. In this study, the plastic events are solely identified based on the non-affine displacement field, which does not explicitly distinguish these different mechanisms. As a result, the rearrangement of groups of atoms can be regarded as the combination of several elementary plastic events. Due to the existence of a high concentration of floppy modes in the flexible system (i.e., 0–40% SiO_2), the reorganizations can be easily triggered under the applied stress, as evidenced by the lowest brittleness in this region (see the green region in Fig. 1d). However, when the rigid cluster is isolated, the crack can always find the path through the region where atoms are not effectively bonded, which results in a low cohesion. In addition, since the connectivity of the atomic network is relatively low, stresses can not effectively be transferred to their neighbors to trigger successive reorganizations (see the illustration in Fig. 4). As a result, even though it features the highest ductility, the dynamic heterogeneity of plastic events (i.e., χ_4 and ξ_4) in the flexible system is not as prominent as compared with the one in the rigid system.

In contrast, for the stressed-rigid system, the atoms are overconstrained and need to overcome a much higher energy barrier to undergo rearrangement under a similar stress state. As a result, we observe the highest brittleness and lowest fracture energy in this region (see the red region in Fig. 1c and d) due to the relatively rare reorganization events during the fracture process. Although the local reorganization can effectively impact its neighbor atoms due to the high network connectivity, the successive reorganizations can hardly be triggered due to the high energy barrier as illustrated in Fig. 4. Thus, the reorganizations are highly localized and result in the lowest values of χ_4 and ξ_4 (see the red

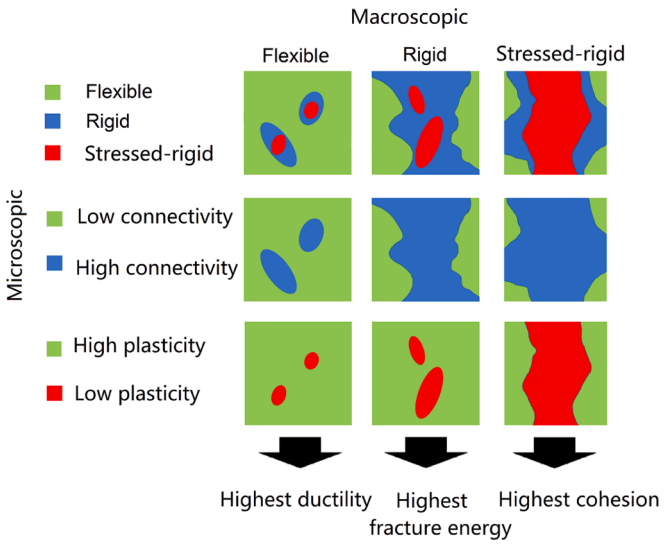

Fig. 4. *Fracture mechanisms controlled by the rigidity transition*. Schematic illustration of the fracture mechanisms under different levels of connectivity. The colors represent the microscopic properties, while each row represents a macroscopic state (i.e., flexible, rigid, or stressed-rigid state).

region in Fig. 3c and e), which finally results in a narrow plastic region (Fig. 1e). However, in the rigid region where only a rigid cluster percolates, the energy barriers caused by the bond constraints are not sufficiently high to prevent a large number of rearrangements triggered by the applied stress. As illustrated in Fig. 4, the isolated low-plasticity regions can hardly prevent large-scale rearrangement and we therefore still observe high ductility in the rigid region (see the blue region in Fig. 1d). Meanwhile, the percolation of rigid clusters forces the crack to propagate through some of the high-cohesive regions, which results in a higher cohesion than that observed in the flexible system. Thus, we observe the highest fracture energy with substantial ductility in this optimal intermediate state. Moreover, the stress caused by the rearrangements can effectively be transferred into the neighboring regions through the connected constraints. As a result, the dynamical heterogeneity becomes more prominent (i.e., high χ_4 and ξ_4) due to the continuous spatial rearrangements. The network heterogeneity of oxide glass and its influence on the mechanical properties can also be described in terms of the ring statistics [52–54].

5. Conclusion

In conclusion, we have investigated the underlying mechanism that controls the ductile-to-brittle transition in aluminosilicate glasses. From the viewpoint of TCT, we show that the percolation of the stressed-rigid cluster is responsible for the dramatic decrease of the fracture energy with composition, while rigid cluster percolation results in the fracture energy anomaly. We find that the observed ductile-to-brittle transition can be understood from the competition between the cohesion (i.e., increase in connectivity) and rearrangements (i.e., decrease in connectivity). The optimized fracture energy can be obtained when the best compromise is achieved. The structural signature for this optimized situation is found in the compositional window where a rigid cluster starts to percolate the system before any stress-rigid cluster percolates. We envision that this finding could guide the design of novel oxide glasses with improved fracture resistance. Furthermore, through the susceptibility and four-point correlation function analyses, we have found that the percolation of the rigid atomic network governs the evolution of susceptibility and the dynamical length of plastic events. The most prominent dynamical heterogeneity can be achieved in the rigid system where the connectivity is low enough to allow for rearrangements and high enough to be able to transfer stresses to neighboring atoms. This result provides new insight into the link between macroscopic ductility, dynamical heterogeneity driven by mechanical stress, and network connectivity of glass.

Declaration of Competing Interest

The authors declare that they have no known competing financial interests or personal relationships that could have appeared to influence the work reported in this paper.

The authors declare the following financial interests/personal relationships which may be considered as potential competing interests

Acknowledgments

M.B. acknowledges funding from the National Science Foundation under Grants DMR-1928538 and DMR-1944510. M.M.S. acknowledges funding from the European Union (ERC, NewGLASS, 101044664). Views and opinions expressed are however those of the author(s) only and do not necessarily reflect those of the European Union or the European Research Council. Neither the European Union nor the granting authority can be held responsible for them.

Supplementary materials

Supplementary material associated with this article can be found, in the online version, at doi:10.1016/j.actamat.2023.118740.

References

[1] X.K. Xi, D.Q. Zhao, M.X. Pan, W.H. Wang, Y. Wu, J.J. Lewandowski, Fracture of brittle metallic glasses: brittleness or plasticity, Phys. Rev. Lett. 94 (2005), 125510, https://doi.org/10.1103/PhysRevLett.94.125510.
[2] J. Schroers, W.L. Johnson, Ductile bulk metallic glass, Phys. Rev. Lett. 93 (2004), 255506, https://doi.org/10.1103/PhysRevLett.93.255506.
[3] J. Pan, Y.P. Ivanov, W.H. Zhou, Y. Li, A.L. Greer, Strain-hardening and suppression of shear-banding in rejuvenated bulk metallic glass, Nature 578 (2020) 559–562, https://doi.org/10.1038/s41586-020-2016-3.
[4] L. Tang, H. Liu, G. Ma, T. Du, N. Mousseau, W. Zhou, M. Bauchy, The energy landscape governs ductility in disordered materials, Mater. Horiz. 8 (2021) 1242–1252, https://doi.org/10.1039/D0MH00980F.
[5] M. Ozawa, L. Berthier, G. Biroli, A. Rosso, G. Tarjus, Random critical point separates brittle and ductile yielding transitions in amorphous materials, PNAS 115 (2018) 6656–6661, https://doi.org/10.1073/pnas.1806156115.
[6] M.L. Falk, J.S. Langer, Deformation and failure of amorphous solidlike materials, Annu. Rev. Condens. Matter Phys. 2 (2011) 353–373, https://doi.org/10.1146/annurev-conmatphys-062910-140452.
[7] A. Nicolas, E.E. Ferrero, K. Martens, J.L. Barrat, Deformation and flow of amorphous solids: insights from elastoplastic models, Rev. Mod. Phys. 90 (2018), 045006, https://doi.org/10.1103/RevModPhys.90.045006.
[8] H. Jia, G. Wang, S. Chen, Y. Gao, W. Li, P.K. Liaw, Fatigue and fracture behavior of bulk metallic glasses and their composites, Prog. Mater. Sci. 98 (2018) 168–248, https://doi.org/10.1016/j.pmatsci.2018.07.002.
[9] J.R. Rice, Dislocation nucleation from a crack tip: an analysis based on the peierls concept, J. Mech. Phys. Solids 40 (1992) 239–271, https://doi.org/10.1016/S0022-5096(05)80012-2.
[10] X. Li, Y. Wei, L. Lu, K. Lu, H. Gao, Dislocation nucleation governed softening and maximum strength in nano-twinned metals, Nature 464 (2010) 877–880, https://doi.org/10.1038/nature08929.
[11] W.T. Read, W. Shockley, Dislocation Models of Crystal Grain Boundaries, Phys. Rev. 78 (1950) 275–289, https://doi.org/10.1103/PhysRev.78.275.
[12] M.L. Falk, J.S. Langer, Dynamics of viscoplastic deformation in amorphous solids, Phys. Rev. E 57 (1998) 7192–7205, https://doi.org/10.1103/PhysRevE.57.7192.
[13] E.D. Cubuk, R.J.S. Ivancic, S.S. Schoenholz, D.J. Strickland, A. Basu, Z.S. Davidson, J. Fontaine, J.L. Hor, Y.R. Huang, Y. Jiang, N.C. Keim, K.D. Koshigan, J.A. Lefever, T. Liu, X.G. Ma, D.J. Magagnosc, E. Morrow, C.P. Ortiz, J.M. Rieser, A. Shavit, T. Still, Y. Xu, Y. Zhang, K.N. Nordstrom, P.E. Arratia, R.W. Carpick, D.J. Durian, Z. Fakhraai, D.J. Jerolmack, D. Lee, J. Li, R. Riggleman, K.T. Turner, A.G. Yodh, D. S. Gianola, A.J. Liu, Structure-property relationships from universal signatures of plasticity in disordered solids, Science 358 (2017) 1033–1037, https://doi.org/10.1126/science.aai8830.
[14] S. Patinet, D. Vandembroucq, M.L. Falk, Connecting local yield stresses with plastic activity in amorphous solids, Phys. Rev. Lett. 117 (2016), 045501, https://doi.org/10.1103/PhysRevLett.117.045501.
[15] R.L. Jack, A.J. Dunleavy, C.P. Royall, Information-theoretic measurements of coupling between structure and dynamics in glass formers, Phys. Rev. Lett. 113 (2014), 095703, https://doi.org/10.1103/PhysRevLett.113.095703.

[16] T. Du, H. Liu, L. Tang, S.S. Sørensen, M. Bauchy, M.M. Smedskjaer, Predicting fracture propensity in amorphous alumina from its static structure using machine learning, ACS Nano 15 (2021) 17705–17716, https://doi.org/10.1021/acsnano.1c05619.
[17] L. Berthier, G. Biroli, Theoretical perspective on the glass transition and amorphous materials, Rev. Mod. Phys. 83 (2011) 587–645, https://doi.org/10.1103/RevModPhys.83.587.
[18] K.A. Kirchner, D.R. Cassar, E.D. Zanotto, M. Ono, S.H. Kim, K. Doss, M.L. Bødker, M.M. Smedskjaer, S. Kohara, L. Tang, M. Bauchy, C.J. Wilkinson, Y. Yang, R. S. Welch, M. Mancini, J.C. Mauro, Beyond the average: spatial and temporal fluctuations in oxide glass-forming systems, Chem. Rev. (2022), https://doi.org/10.1021/acs.chemrev.1c00974.
[19] H. Tanaka, T. Kawasaki, H. Shintani, K. Watanabe, Critical-like behaviour of glass-forming liquids, Nat. Mater. 9 (2010) 324–331, https://doi.org/10.1038/nmat2634.
[20] O. Dauchot, G. Marty, G. Biroli, Dynamical heterogeneity close to the jamming transition in a sheared granular material, Phys. Rev. Lett. 95 (2005), 265701, https://doi.org/10.1103/PhysRevLett.95.265701.
[21] A.S. Keys, A.R. Abate, S.C. Glotzer, D.J. Durian, Measurement of growing dynamical length scales and prediction of the jamming transition in a granular material, Nat. Phys. 3 (2007) 260–264, https://doi.org/10.1038/nphys572.
[22] J.C. Phillips, Topology of covalent non-crystalline solids I: short-range order in chalcogenide alloys, J. Non Cryst. Solids 34 (1979) 153–181, https://doi.org/10.1016/0022-3093(79)90033-4.
[23] J.C. Phillips, Topology of covalent non-crystalline solids II: medium-range order in chalcogenide alloys and ASi(Ge), J. Non Cryst. Solids 43 (1981) 37–77, https://doi.org/10.1016/0022-3093(81)90172-1.
[24] M.F. Thorpe, Continuous deformations in random networks, J. Non Cryst. Solids 57 (1983) 355–370, https://doi.org/10.1016/0022-3093(83)90424-6.
[25] J.C. Maxwell, L. on the calculation of the equilibrium and stiffness of frames, Lond. Edinb. Dublin Philos. Mag. J. Sci. 27 (1864) 294–299, https://doi.org/10.1080/14786446408643668.
[26] G.G. Naumis, Energy landscape and rigidity, Phys. Rev. E 71 (2005), 026114, https://doi.org/10.1103/PhysRevE.71.026114.
[27] F. Wang, S. Mamedov, P. Boolchand, B. Goodman, M. Chandrasekhar, Pressure raman effects and internal stress in network glasses, Phys. Rev. B 71 (2005), 174201, https://doi.org/10.1103/PhysRevB.71.174201.
[28] M.V. Chubynsky, M.A. Brière, N. Mousseau, Self-organization with equilibration: a model for the intermediate phase in rigidity percolation, Phys. Rev. E 74 (2006), 016116, https://doi.org/10.1103/PhysRevE.74.016116.
[29] S. Chakravarty, D.G. Georgiev, P. Boolchand, M. Micoulaut, Ageing, fragility and the reversibility window in bulk alloy glasses, J. Phys. Condens. Matter 17 (2004) L1–L7, https://doi.org/10.1088/0953-8984/17/1/L01.
[30] M. Bauchy, B. Wang, M. Wang, Y. Yu, M.J. Abdolhosseini Qomi, M.M. Smedskjaer, C. Bichara, F.J. Ulm, R. Pellenq, Fracture toughness anomalies: viewpoint of topological constraint theory, Acta Mater. 121 (2016) 234–239, https://doi.org/10.1016/j.actamat.2016.09.004.
[31] M. Bauchy, M. Micoulaut, Transport anomalies and adaptative pressure-dependent topological constraints in tetrahedral liquids: evidence for a reversibility window analogue, Phys. Rev. Lett. 110 (2013), 095501, https://doi.org/10.1103/PhysRevLett.110.095501.
[32] M. Bauchy, M. Micoulaut, M. Boero, C. Massobrio, Compositional thresholds and anomalies in connection with stiffness transitions in network glasses, Phys. Rev. Lett. 110 (2013), 165501, https://doi.org/10.1103/PhysRevLett.110.165501.
[33] M.M. Smedskjaer, J.C. Mauro, Y. Yue, Prediction of glass hardness using temperature-dependent constraint theory, Phys. Rev. Lett. 105 (2010), 115503, https://doi.org/10.1103/PhysRevLett.105.115503.
[34] M. Bauchy, M.J.A. Qomi, C. Bichara, F.J. Ulm, R.J.M. Pellenq, Rigidity transition in materials: hardness is driven by weak atomic constraints, Phys. Rev. Lett. 114 (2015), 125502, https://doi.org/10.1103/PhysRevLett.114.125502.
[35] P. Ball, Concrete mixing for gorillas, Nature Mater 14 (2015), https://doi.org/10.1038/nmat4279, 472–472.
[36] J.C. Mauro, A.J. Ellison, L.D. Pye, Glass: the nanotechnology connection, Int. J. Appl. Glass Sci. 4 (2013) 64–75, https://doi.org/10.1111/ijag.12030.
[37] J.C. Mauro, M.M. Smedskjaer, Unified physics of stretched exponential relaxation and weibull fracture statistics, Phys. A Stat. Mech. Appl. 391 (2012) 6121–6127, https://doi.org/10.1016/j.physa.2012.07.013.
[38] B. Wang, Y. Yu, M. Wang, J.C. Mauro, M. Bauchy, Nanoductility in silicate glasses is driven by topological heterogeneity, Phys. Rev. B 93 (2016), 064202, https://doi.org/10.1103/PhysRevB.93.064202.
[39] S. Nosé, A unified formulation of the constant temperature molecular dynamics methods, J. Chem. Phys. 81 (1984) 511–519, https://doi.org/10.1063/1.447334.
[40] W.G. Hoover, Canonical dynamics: equilibrium phase-space distributions, Phys. Rev. A 31 (1985) 1695–1697, https://doi.org/10.1103/PhysRevA.31.1695.
[41] N. Jakse, M. Bouhadja, J. Kozaily, J.W.E. Drewitt, L. Hennet, D.R. Neuville, H. E. Fischer, V. Cristiglio, A. Pasturel, Interplay between non-bridging oxygen, triclusters, and fivefold Al coordination in low silica content calcium aluminosilicate melts, Appl. Phys. Lett. 101 (2012), 201903, https://doi.org/10.1063/1.4766920.
[42] M. Bauchy, Structural, vibrational, and elastic properties of a calcium aluminosilicate glass from molecular dynamics simulations: the role of the potential, J. Chem. Phys. 141 (2014), 024507, https://doi.org/10.1063/1.4886421.
[43] S. Plimpton, Fast parallel algorithms for short-range molecular dynamics, J. Comput. Phys. 117 (1995) 1–19, https://doi.org/10.1006/jcph.1995.1039.
[44] B. Wang, Y. Yu, Y.J. Lee, M. Bauchy, Intrinsic nano-ductility of glasses: the critical role of composition, Front. Mater. 2 (2015), https://doi.org/10.3389/fmats.2015.00011.
[45] L. Berthier, Dynamic heterogeneity in amorphous materials, Phys. Coll. Park Md 4 (2011) 42, https://doi.org/10.1103/Physics.4.42.
[46] N. Lačević, F.W. Starr, T.B. Schrøder, V.N. Novikov, S.C. Glotzer, Growing correlation length on cooling below the onset of caging in a simulated glass-forming liquid, Phys. Rev. E 66 (2002), 030101, https://doi.org/10.1103/PhysRevE.66.030101.
[47] C.E. Maloney, Amorphous systems in athermal, quasistatic shear, Phys. Rev. E (2006) 74, https://doi.org/10.1103/PhysRevE.74.016118.
[48] N. Lačević, F.W. Starr, T.B. Schrøder, S.C. Glotzer, Spatially heterogeneous dynamics investigated via a time-dependent four-point density correlation function, J. Chem. Phys. 119 (2003) 7372–7387, https://doi.org/10.1063/1.1605094.
[49] T. To, S.S. Sørensen, J.F.S. Christensen, R. Christensen, L.R. Jensen, M. Bockowski, M. Bauchy, M.M. Smedskjaer, Bond switching in densified oxide glass enables record-high fracture toughness, ACS Appl. Mater. Interfaces. 13 (2021) 17753–17765, https://doi.org/10.1021/acsami.1c00435.
[50] F. Bamer, S.S. Alshabab, A. Paul, F. Ebrahem, B. Markert, B. Stamm, Data-driven classification of elementary rearrangement events in silica glass, Scr. Mater. 205 (2021), 114179, https://doi.org/10.1016/j.scriptamat.2021.114179.
[51] S. Bonfanti, R. Guerra, C. Mondal, I. Procaccia, S. Zapperi, Elementary plastic events in amorphous silica, Phys. Rev. E 100 (2019), 060602, https://doi.org/10.1103/PhysRevE.100.060602.
[52] F. Ebrahem, F. Bamer, B. Markert, The influence of the network topology on the deformation and fracture behaviour of silica glass: a molecular dynamics study, Comput. Mater. Sci. 149 (2018) 162–169, https://doi.org/10.1016/j.commatsci.2018.03.017.
[53] F. Bamer, F. Ebrahem, B. Markert, Plasticity in vitreous silica induced by cyclic tension considering rate-dependence: role of the network topology, J. Non Cryst. Solids 503–504 (2019) 176–181, https://doi.org/10.1016/j.jnoncrysol.2018.09.043.
[54] F. Ebrahem, F. Bamer, B. Markert, Vitreous 2D silica under tension: from brittle to ductile behaviour, Mater. Sci. Eng. A 780 (2020), 139189, https://doi.org/10.1016/j.msea.2020.139189.